LETTER

doi:10.1038/nature12899

# Skin pigmentation provides evidence of convergent melanism in extinct marine reptiles

Johan Lindgren[1], Peter Sjövall[2], Ryan M. Carney[3], Per Uvdal[4,5], Johan A. Gren[1], Gareth Dyke[6,7], Bo Pagh Schultz[8], Matthew D. Shawkey[9], Kenneth R. Barnes[10] & Michael J. Polcyn[11]

**Throughout the animal kingdom, adaptive colouration serves critical functions ranging from inconspicuous camouflage to ostentatious sexual display, and can provide important information about the environment and biology of a particular organism[1,2]. The most ubiquitous and abundant pigment, melanin, also has a diverse range of non-visual roles, including thermoregulation in ectotherms[3,4]. However, little is known about the functional evolution of this important biochrome through deep time, owing to our limited ability to unambiguously identify traces of it in the fossil record[2]. Here we present direct chemical evidence of pigmentation in fossilized skin, from three distantly related marine reptiles: a leatherback turtle[5], a mosasaur[6] and an ichthyosaur[7]. We demonstrate that dark traces of soft tissue in these fossils are dominated by molecularly preserved eumelanin, in intimate association with fossilized melanosomes. In addition, we suggest that contrary to the countershading of many pelagic animals[8,9], at least some ichthyosaurs were uniformly dark-coloured in life. Our analyses expand current knowledge of pigmentation in fossil integument beyond that of feathers[2,10], allowing for the reconstruction of colour over much greater ranges of extinct taxa and anatomy. In turn, our results provide evidence of convergent melanism in three disparate lineages of secondarily aquatic tetrapods. Based on extant marine analogues, we propose that the benefits of thermoregulation and/or crypsis are likely to have contributed to this melanisation, with the former having implications for the ability of each group to exploit cold environments.**

On rare occasions, the fossil record reveals examples of exceptional preservation, in which decay-prone tissues, such as skin, are preserved as 'an organic film'[11] with a high degree of morphological fidelity. These specimens provide information crucial to our understanding of ancient anatomy and evolutionary patterns. For example, the discovery of a dark-coloured 'halo' surrounding the skeleton of extraordinarily preserved ichthyosaurs (an extinct group of ocean-going reptiles[7]) in the 1890s drastically changed the prevailing image of these animals, revealing their remarkably derived, piscine body plan. Likewise, the preservation of carbonised scales in mosasaurs (another lineage of Mesozoic-era marine reptiles[6]) has greatly improved our understanding of how these ancient lizards evolved from land dwellers to pelagic cruisers[12].

Although such fossils have advanced our knowledge of the body plans of these animals, the origin and composition of the dark matter that forms preserved surface structures have yet to be resolved. Previous studies have shown that carbonised fossil 'skin' is rich in micrometre-sized spherical to rod-shaped bodies[13]. Morphologically, these structures resemble melanosomes (lysosome-related pigment organelles) but also microbes, and thus there has been debate over whether they represent fossilized remains of endogenous organelles[10,14] or bacteria[7,13].

Therefore, to elucidate the molecular composition of putative fossilized skin, we analysed samples from three phylogenetically diverse marine reptiles—a 55-Myr-old leatherback turtle (FUM-N-1450; MUSERUM), an 86-Myr-old mosasaur (SMU 76532; Shuler Museum of Paleontology) and a 196–190-Myr-old ichthyosaur (YORYM 1993.338; Yorkshire Museum) (Figs 1–4; see Supplementary Information)—using time-of-flight secondary ion mass spectrometry (ToF-SIMS) and scanning electron microscopy (SEM). ToF-SIMS provides detailed information on the composition and spatial distribution of surface molecules and chemical structures[15,16]. In the three specimens, soft tissue anatomy associated with the skeletal elements is preserved as macroscopically amorphous, matt black material; however, SEM reveals masses of ovoid bodies, with long and short axes of approximately $0.8 \times 0.5$ μm (turtle; Fig. 2b, c), $0.5 \times 0.3$ μm (mosasaur; Fig. 3b, c) and $0.8 \times 0.5$ μm (ichthyosaur; Fig. 4b, c) (Supplementary Information). These dimensions are consistent with those of melanosomes from extant lizards[17] and bird feathers[10]. Energy-dispersive X-ray (EDX) microanalysis shows that carbon in these specimens is associated with the 'skin' but not the adjacent sedimentary matrix, suggesting that the former represents organic residues (Extended Data Fig. 1).

ToF-SIMS analysis produced negative-ion mass spectra from specific sample regions that closely match the spectrum obtained from natural eumelanin (Figs 2d, 3d and 4d and Extended Data Figs 2 and 3), indicating the presence of considerable amounts of this black to brown biochrome on the sampled surfaces. All relevant features of the standard

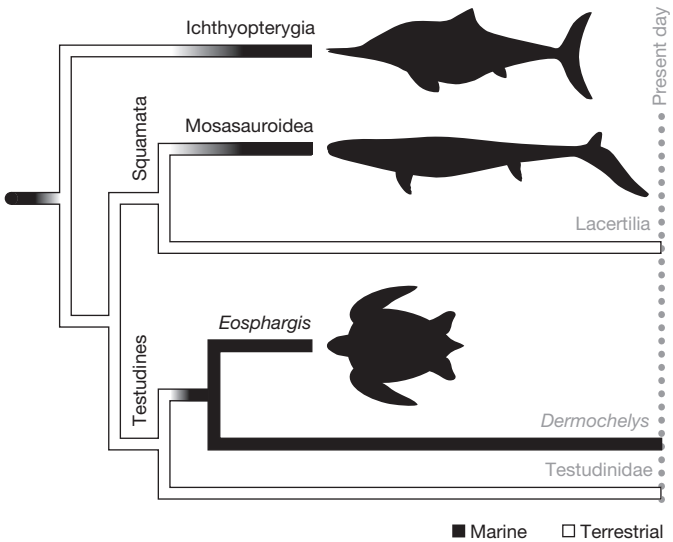


**Figure 1 | Phylogenetic relationships of the three fossil marine reptiles examined in this study.** Note that each lineage independently became secondarily aquatic (black branches, marine; white branches, terrestrial). Phylogeny is based on ref. 26; branch lengths and body sizes are not to respective scale.

[1]Department of Geology, Lund University, SE-223 62 Lund, Sweden. [2]SP Technical Research Institute of Sweden, Chemistry, Materials and Surfaces, SE-501 15 Borås, Sweden. [3]Department of Ecology and Evolutionary Biology, Brown University, Providence, Rhode Island 02906, USA. [4]MAX-IV laboratory, Lund University, SE-221 00 Lund, Sweden. [5]Chemical Physics, Department of Chemistry, Lund University, SE-221 00 Lund, Sweden. [6]Ocean and Earth Sciences, University of Southampton, Southampton SO14 3ZH, UK. [7]Institute for Life Sciences, University of Southampton, Southampton SO14 3ZH, UK. [8]MUSERUM, Natural History Division, Havnevej 14, 7800 Skive, Denmark. [9]Integrated Bioscience Program, University of Akron, Akron, Ohio 44325, USA. [10]Mosasaur Ranch Museum, Lajitas, Texas 79852, USA. [11]Roy M. Huffington Department of Earth Sciences, Southern Methodist University, Dallas, Texas 75275, USA.

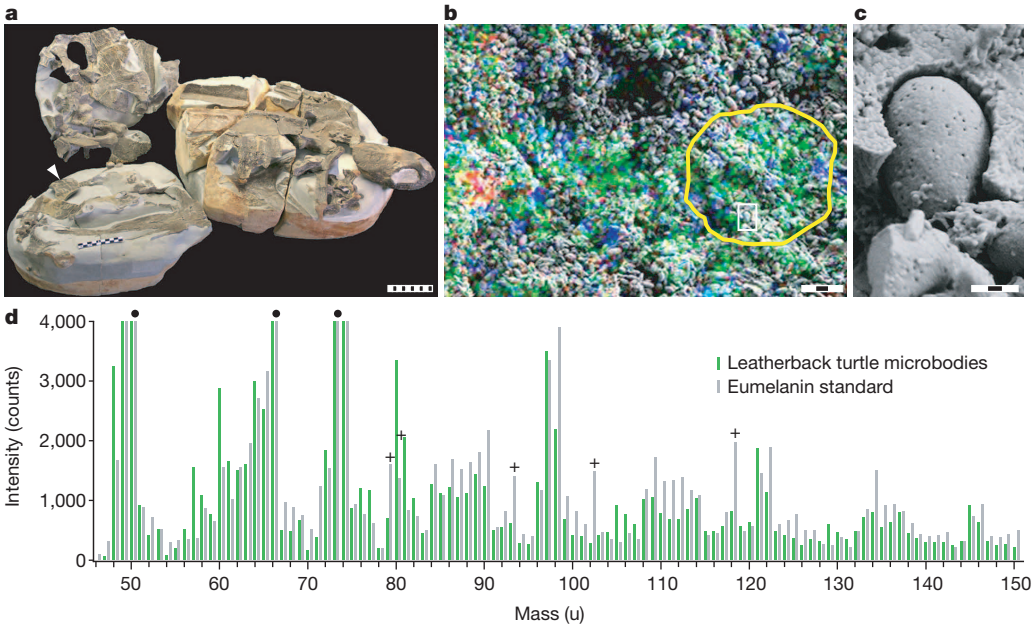


**Figure 2 | SEM and ToF-SIMS data of fossil leatherback turtle FUM-N-1450. a**, Photograph of specimen. Sampled skin structures are marked with an arrowhead. Scale bar, 10 cm. **b**, A semi-transparent ion image showing the spatial distribution of peaks characteristic of eumelanin (green; see Methods), silicon oxide (blue) and sulphate (red) superimposed onto a SEM image of the 'skin'. Scale bar, 3 μm. **c**, Enlargement of the demarcated area in **b** (white box) showing a melanosome-like microbody. Scale bar, 300 nm. **d**, Negative-ion ToF-SIMS spectra from the area demarcated by a yellow line in **b** ('Leatherback turtle microbodies') and natural eumelanin. Filled circles (above grey bars) indicate peaks used to produce the eumelanin ion image in **b**, and plus symbols (above grey bars) indicate peaks from inorganic ions that are not part of the eumelanin structure (see Methods for further discussion). u, unified atomic mass unit.

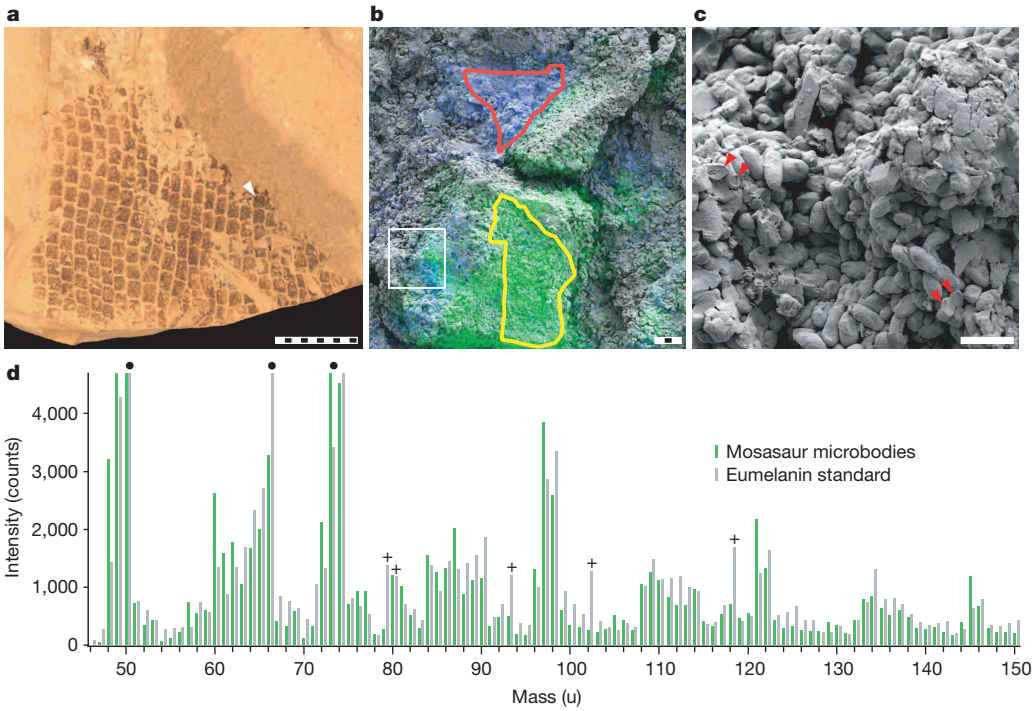


**Figure 3 | SEM and ToF-SIMS data of mosasaur SMU 76532. a**, Photograph of section with 'scales'. Arrowhead indicates analysed area. Scale bar, 10 mm. **b**, A semi-transparent ion image showing the spatial distribution of peaks characteristic of eumelanin (green; see Methods) and silicon oxide (blue) superimposed onto a SEM image of the 'scales'. The yellow line demarcates the area from which the spectrum presented in **d** ('Mosasaur microbodies') was collected, whereas the red line demarcates the area from which the upper spectrum in Extended Data Fig. 3 was collected. Scale bar, 3 μm. **c**, Enlargement of the demarcated area in **b** (white box) showing melanosome-like microbodies (arrowheads indicate solid interior; see Supplementary Information). Scale bar, 1 μm. **d**, Negative-ion ToF-SIMS spectra from the area demarcated by a yellow line in **b** and natural eumelanin. Filled circles (above grey bars) indicate peaks used to produce the eumelanin ion image in **b**, and plus symbols (above grey bars) indicate peaks from inorganic ions that are not part of the eumelanin structure (see Methods for further discussion).

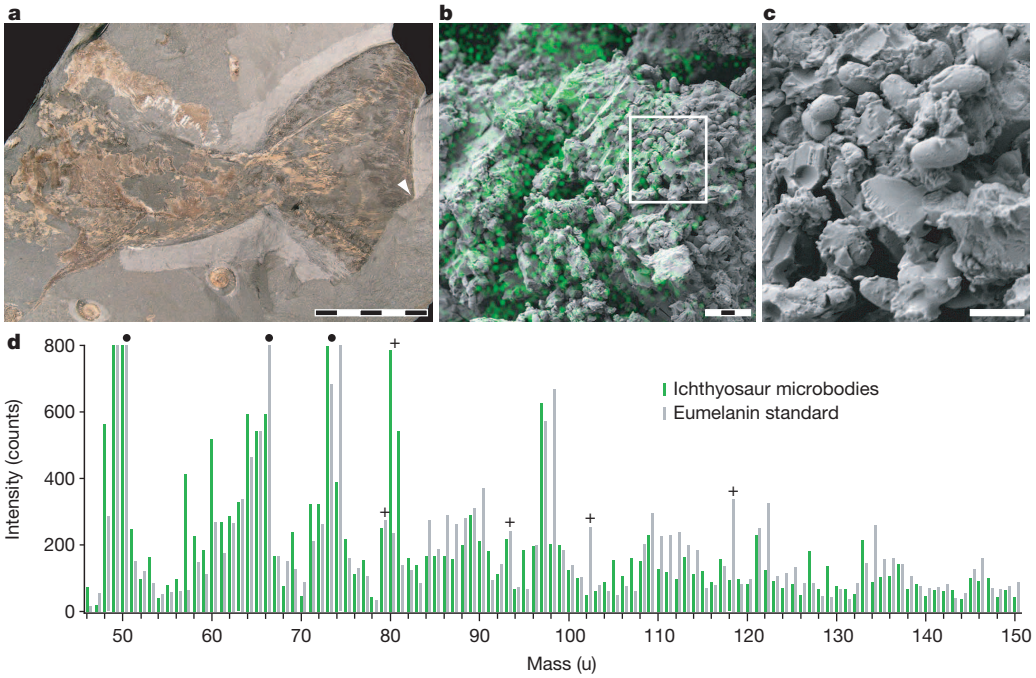


**Figure 4 | SEM and ToF-SIMS data of ichthyosaur YORYM 1993.338.** **a**, Photograph of specimen (caudal region and tail fin). The analysed area is indicated by an arrowhead. Scale bar, 5 cm. **b**, A semi-transparent ion image showing the spatial distribution of peaks characteristic of eumelanin (green; see Methods) superimposed onto a SEM image of the 'skin'. Scale bar, 3 μm. **c**, Enlargement of the demarcated area in **b** (white box) showing melanosome-like microbodies. Scale bar, 1 μm. **d**, Negative-ion ToF-SIMS spectra of the 'skin' and natural eumelanin. Filled circles (above grey bars) indicate peaks used to produce the ion image in **b**, and plus symbols (above grey bars) indicate peaks from inorganic ions that are not part of the eumelanin structure (see Methods for further discussion).

spectrum are reproduced in the fossil spectra, including relative intensity distributions and precise peak positions (measured at 'high' mass resolution; see Extended Data Table 1) of all major peaks occurring at 49, 50, 66, 73, 74, 97, 98, 121, 122, 145, and 146 u (unified atomic mass unit), as well as several less intense peaks in the entire mass range up to 175 u. Moreover, all main eumelanin peaks show the same spatial distribution, demonstrating that they originate from the same molecular species (Extended Data Fig. 4). Importantly, superimposition of these data onto SEM micrographs shows that the eumelanin peaks from all three fossil specimens consistently appear in intimate association with melanosome-like microbodies (Figs 2b, 3b and 4b). Additional peaks representing other molecular structures, including silica (60, 76 and 77 u) and sulphate (80 u), display distinctly different spatial distributions not associated with melanin or the microbodies (Figs 2b and 3b and Extended Data Fig. 4).

The other main class of melanin pigment is phaeomelanin, which imparts red to yellow colours[18]. For a long time phaeomelanin was thought to be absent outside of mammals and birds, but it has recently been identified in Testudines[18]; phaeomelanosomes have also been found to fossilize[10]. However, the spectra from our three specimens do not indicate large amounts of phaeomelanin (Extended Data Fig. 5), and the ovoid microbodies are inconsistent with the spherical morphology of phaeomelanosomes[10]. Although minor contributions from compounds, such as phaeomelanin, cannot be excluded given the presence of sulphur (Extended Data Figs 4 and 6), the latter is likely to be diagenetic in origin (Supplementary Information). Ultimately, our molecular and imaging analyses provide compelling evidence that the organic content of the structures forming the 'skin' in all three specimens is dominated by eumelanin, and that the structures themselves represent fossilized melanosomes (see also Supplementary Information).

The fossil spectra are also inconsistent with those taken from three microbial mat samples[16], as well as from nine molecular standards consisting of two compounds that are structurally similar to melanin, three porphyrin pigments, and four compounds that comprise the three other types of colour-producing cells (chromatophores) found in reptilian integument: erythrophores, iridophores and xanthophores (Extended Data Figs 5 and 6; Supplementary Information)[17]. However, given that the relative preservation potential of non-melanic pigments and structural colour-producing chromatophores is believed to be relatively low[2], their absence may not necessarily indicate lack of original presence. Nevertheless, a relationship exists between melanin density and skin darkness[3,17,19], and the soft tissues in the fossil specimens are composed entirely of tightly packed melanosomes. Therefore, we conclude that the bodies of the three marine reptiles represented by these fossils originally had, at least partially, eumelanic colouration similar to the extant leatherback turtle, *Dermochelys coriacea* (Extended Data Fig. 7)[5].

Given that animal pigmentation is subject to natural selection[1], the integumental melanisation we report was likely to have been advantageous to these organisms in life. One well-known modern example is thermal melanism, which provides faster heating and higher equilibrium temperatures through increased absorption of solar radiation due to lower albedo[3,4]. This adaptation has been found to increase the fitness of various organisms in cold climates, including reptiles[3,4]. Among extant reptiles, the leatherback turtle has the largest geographical and temperature ranges, including near-freezing waters in the Arctic Circle[5,20]. The leatherback's ability to maintain a high core body temperature is generally attributed to an integrated suite of physiological and behavioural adaptations, including extremely large body size (gigantothermy)[5,20]. It has also been suggested that the dark dorsal colouring of leatherbacks, coupled with their routinely observed, apparent basking behaviour, maximizes absorption of solar radiation[21], and studies of leatherbacks foraging at high latitudes have revealed that these turtles surface for extended periods of time during daylight hours (peaking at around midday)[5,21]. Furthermore, experimental results demonstrate that the black dorsal colouration of hatchlings of the related green sea turtle, *Chelonia mydas*, has an important role in elevating body temperature; this in turn is believed to increase growth rates during this vulnerable life history stage[22]. Thus, such thermal melanism presumably also has a role in leatherback turtles, particularly given that they inhabit colder environments (at

least as sub-adults and adults[5]) and exhibit the fastest growth rates of any living turtle[23]. Adult leatherbacks also retain this black colouration—unlike adult green sea turtles[22] and despite lower growth rates compared to their juvenile stage[23]—which may be due in part to thermal selective pressure throughout ontogeny. In addition, results from physical and theoretical modelling predict more advantageous thermal melanism in larger organisms[3].

It is therefore feasible that selective pressures for fast growth, large size and/or homeothermy also selected for melanisation in extant (and fossil) leatherbacks. It is interesting to note that Eocene-epoch leatherback turtles also ranged into cold, high-latitude climates[24], and thus presumably possessed thermoregulatory adaptations comparable to those found in extant *Dermochelys*. Similar selective pressures are likely to have acted on mosasaurs and ichthyosaurs as well, both of which were fast-growing, large and homeothermic[25,26]. This homeothermy, which is likely to have been augmented by the thermal advantages of melanised skin during the sea-surfacing behaviours of these obligate air-breathers, allowed exploitation of ecological niches near the Arctic and Antarctic[24,25,27].

Pigmentation is often a multi-functional trait[1,2], and thus may have performed other non-mutually-exclusive roles, such as camouflage. For example, in addition to thermoregulation, the black colouration of green sea turtle hatchlings provides countershading (a dark dorsum and light ventrum), a simple but effective form of concealment against predators above, and below, the water surface[22]. Many other living aquatic organisms are countershaded[9,22], including *Dermochelys*[5], and this is occasionally also observed in exceptionally preserved fossils[8]. However, assuming that the black body outlines of ichthyosaur fossils with a full 'skin' envelope (Extended Data Fig. 8) represent endogenous pigments and/or organelles as reported here in YORYM 1993.338, we infer that these animals were uniformly dark-coloured in life. Some extant marine animals, including the deep diving sperm whale, *Physeter macrocephalus*, have a uniform dark colouration, and it has been suggested that this colour scheme acts as background matching in low light environments[9]. Although this is not a statistically supported association among cetaceans[9], such a function in ichthyosaurs would nonetheless be consistent with their inferred deep diving habits[7]. The particular distribution of dark and light pigments in mosasaurs is unknown; however, the keeled scales present in some forms would have reduced shininess and provided a non-reflective appearance[12]. Similarly, we reason that both cryptic and thermal melanism in marine reptiles would tend to select against other types of chromatophores and structural colouration, which by their nature serve to reflect light. This is consistent with the matt black appearance of extant leatherback skin, which is also smooth in adults due to a lack of scales[5], a feature believed to be shared by at least some derived ichthyosaurs[7,11]. More speculative functions for the melanisation observed in these three fossil taxa include photoprotection from the continuous exposure to ultraviolet radiation while at the sea surface[28], and mechanical strengthening of the integumentary tissue[29]; gene(s) responsible for the melanisation may also have had pleiotropic effects on other physiological or behavioural traits, such as increased aggressiveness[30].

Ultimately, our molecular approach provides an unprecedented level of confidence for the detection and characterization of pigment in fossilized integument. Furthermore, the ability to reconstruct colour in skin has great potential for a phylogenetically diverse range of fossil animals. Our results suggest that dark colouration in extinct marine reptiles may be common, as it is in extant marine amniotes[5,9]; such convergence reflects the important evolutionary role that melanin played after each of these ancient reptile lineages returned to the sea.

## METHODS SUMMARY

**Preparation of samples.** Small tissue samples were removed from each specimen using a sterile scalpel and rinsed multiple times in 96% ethanol and 'ultrapure' (Milli-Q) water, dried under a hood, and wrapped in aluminium foil until examination. Prior to ToF-SIMS analysis, the surface of each sample was partially removed using a sterile scalpel, and the collected material was deposited on double-sided cellophane tape. Aluminium foil was used to cover all work areas, and surgical gloves were used in all handling of the 'skin' samples. Treatment of modern reference samples was identical to that of the fossil structures for all analyses.

**Scanning electron microscopy.** Initial screening was performed using a Hitachi S-3400N SEM on uncoated samples under low vacuum, and the elemental composition was determined via elemental mapping using EDX analysis (1,900 s scanning time at 15 keV, 62.0 μA and a working distance of 10 mm). After ToF-SIMS analysis, the samples were sputter-coated with gold and re-examined using a Zeiss Supra 40VP scanning electron microscope (2 keV, working distance 3–5 mm, Everhart-Thornley secondary electron detector).

**Time-of-flight secondary ion mass spectrometry.** ToF-SIMS analyses in the static SIMS mode were performed in a ToF-SIMS IV instrument (IONTOF GmbH) using 25 keV $Bi_3^+$ primary ions and low energy electron flooding for charge compensation. High mass resolution data ($m/\Delta m$ ~5,000) were acquired at a spatial resolution of ~3–4 μm, whereas high image resolution data (spatial resolution ~0.2–0.5 μm) were obtained at a mass resolution of $m/\Delta m$ ~300; in both cases at 256 × 256 pixels. Because the positive-ion spectra were found to show strong interference with the signal from the sedimentary matrix, only negative-ion data are presented here.

**Online Content** Any additional Methods, Extended Data display items and Source Data are available in the online version of the paper; references unique to these sections appear only in the online paper.

**Received 9 October; accepted 22 November 2013.**
**Published online 8 January 2014.**

1. Hubbard, J. K., Uy, J. A. C., Hauber, M. E., Hoekstra, H. E. & Safran, R. J. Vertebrate pigmentation: from underlying genes to adaptive function. *Trends Genet.* **26,** 231–239 (2010).
2. McNamara, M. E. The taphonomy of colour in fossil insects and feathers. *Palaeontology* **56,** 557–575 (2013).
3. Clusella Trullas, S., van Wyk, J. H. & Spotila, J. R. Thermal melanism in ectotherms. *J. Therm. Biol.* **32,** 235–245 (2007).
4. Clusella Trullas, S., van Wyk, J. H. & Spotila, J. R. Thermal benefits of melanism in cordylid lizards: a theoretical and field test. *Ecology* **90,** 2297–2312 (2009).
5. Eckert, K. L., Wallace, B. P., Frazier, J. G., Eckert, S. A. & Pritchard, P. C. H. *Synopsis of the Biological Data on the Leatherback Sea Turtle* (Dermochelys coriacea) (US Department of Interior, Fish and Wildlife Service, 2012).
6. Lindgren, J., Kaddumi, H. F. & Polcyn, M. J. Soft tissue preservation in a fossil marine lizard with a bilobed tail fin. *Nature Commun.* **4,** 2423 (2013).
7. Motani, R. Evolution of fish-shaped reptiles (Reptilia: Ichthyopterygia) in their physical environments and constraints. *Annu. Rev. Earth Planet. Sci.* **33,** 395–420 (2005).
8. Gottfried, M. D. Earliest fossil evidence for protective pigmentation in an actinopterygian fish. *Hist. Biol.* **3,** 79–83 (1989).
9. Caro, T., Beeman, K., Stankowich, T. & Whitehead, H. The functional significance of colouration in cetaceans. *Evol. Ecol.* **25,** 1231–1245 (2011).
10. Li, Q. *et al.* Plumage color patterns of an extinct dinosaur. *Science* **327,** 1369–1372 (2010).
11. Martill, D. M. An ichthyosaur with preserved soft tissue from the Sinemurian of southern England. *Palaeontology* **38,** 897–903 (1995).
12. Lindgren, J., Alwmark, C., Caldwell, M. W. & Fiorillo, A. R. Skin of the Cretaceous mosasaur *Plotosaurus*: implications for aquatic adaptations in giant marine reptiles. *Biol. Lett.* **5,** 528–531 (2009).
13. Martill, D. M. Prokaryote mats replacing soft tissues in Mesozoic marine reptiles. *Mod. Geol.* **11,** 265–269 (1987).
14. Whitear, M. On the colour of an ichthyosaur. *Ann. Mag. Nat. Hist.* **9,** 742–744 (1956).
15. Thiel, V. & Sjövall, P. Using time-of-flight secondary ion mass spectrometry to study biomarkers. *Annu. Rev. Earth Planet. Sci.* **39,** 125–156 (2011).
16. Lindgren, J. *et al.* Molecular preservation of the pigment melanin in fossil melanosomes. *Nature Commun.* **3,** 824 (2012).
17. Kuriyama, T., Miyaji, K., Sugimoto, M. & Hasegawa, M. Ultrastructure of the dermal chromatophores in a lizard (Scincidae: *Plestiodon latiscutatus*) with conspicuous body and tail coloration. *Zoolog. Sci.* **23,** 793–799 (2006).
18. Roulin, A., Mafli, A. & Wakamatsu, K. Reptiles produce pheomelanin: evidence in the eastern Hermann's tortoise (*Eurotestudo boettgeri*). *J. Herpetol.* **47,** 258–261 (2013).
19. Rosenblum, E. B., Hoekstra, H. E. & Nachman, M. W. Adaptive reptile color variation and the evolution of the *Mc1r* gene. *Evolution* **58,** 1794–1808 (2004).
20. Bostrom, B. L., Jones, T. T., Hastings, M. & Jones, D. R. Behaviour and physiology: the thermal strategy of leatherback turtles. *PLoS ONE* **5,** e13925 (2010).
21. James, M. C., Myers, R. A. & Ottensmeyer, C. A. Behaviour of leatherback sea turtles, *Dermochelys coriacea*, during the migratory cycle. *Proc. R. Soc. Lond. B* **272,** 1547–1555 (2005).
22. Bustard, H. R. The adaptive significance of coloration in hatchling green sea turtles. *Herpetologica* **26,** 224–227 (1970).

23. Zug, G. R. & Parham, J. F. Age and growth in leatherback turtles, *Dermochelys coriacea* (Testudines: Dermochelyidae): a skeletochronological analysis. *Chelonian Conserv. Biol.* **2,** 244–249 (1996).
24. Albright, L. B., Woodburne, M. O., Case, J. A. & Chaney, D. S. A leatherback sea turtle from the Eocene of Antarctica: implications for antiquity of gigantothermy in Dermochelyidae. *J. Vertebr. Paleontol.* **23,** 945–949 (2003).
25. Bernard, A. *et al.* Regulation of body temperature by some Mesozoic marine reptiles. *Science* **328,** 1379–1382 (2010).
26. Houssaye, A. Bone histology of aquatic reptiles: what does it tell us about secondary adaptation to an aquatic life? *Biol. J. Linn. Soc.* **108,** 3–21 (2013).
27. Rich, T. H., Vickers-Rich, P. & Gangloff, R. A. Polar dinosaurs. *Science* **295,** 979–980 (2002).
28. Martinez-Levasseur, L. M. *et al.* Whales use distinct strategies to counteract solar ultraviolet radiation. *Sci. Rep.* **3,** 2386 (2013).
29. McGraw, K. J. in *Bird Coloration* Vol. 1 (eds Hill, G. E. & McGraw, K. J.) 243–294 (Harvard Univ. Press, 2006).
30. Ducrest, A.-L., Keller, L. & Roulin, A. Pleiotropy in the melanocortin system, coloration and behavioural syndromes. *Trends Ecol. Evol.* **23,** 502–510 (2008).

**Supplementary Information** is available in the online version of the paper.

**Acknowledgements** We thank I. Gladstone, S. King and the Yorkshire Museum for permission to sample YORYM 1993.338, as well as J. Wyneken, P. Weston and L. Alibardi for providing and sectioning the extant leatherback turtle skin samples, respectively. B. P. Kear took the photograph of PMU R435 (Extended Data Fig. 8). This research was supported by grants from the Swedish Research Council, the Crafoord Foundation, the Royal Swedish Academy of Sciences (J.L.), VINNOVA Swedish Governmental Agency for Innovation Systems (P.S.), the National Geographic Society/Waitt Foundation (R.M.C.), the National Science Foundation, Human Frontiers Science Program, and Air Force Office of Scientific Research (M.D.S.).

**Author Contributions** J.L. designed the project. J.L., P.S., R.M.C. and G.D. wrote the manuscript. J.L., P.S., R.M.C., J.A.G. and P.U. prepared the images. G.D., B.P.S., M.D.S., K.R.B. and M.J.P. provided materials, observations and scientific interpretations. All authors discussed the results and provided input on the manuscript.

**Author Information** Reprints and permissions information is available at www.nature.com/reprints. The authors declare no competing financial interests. Readers are welcome to comment on the online version of the paper. Correspondence and requests for materials should be addressed to J.L. (johan.lindgren@geol.lu.se).

## METHODS

**Preparation of samples.** Small tissue samples were removed from each specimen using a sterile scalpel and rinsed multiple times in 96% ethanol and 'ultrapure' (Milli-Q) water, dried under a hood, and wrapped in aluminium foil until examination. Prior to ToF-SIMS analysis, the surface of each sample was partially removed using a sterile scalpel, and the collected material was deposited on double-sided cellophane tape. Aluminium foil was used to cover all work areas, and surgical gloves were used in all handling of the 'skin' samples. Treatment of modern reference samples was identical to that of the fossil structures for all analyses.

**Scanning electron microscopy.** Initial screening was performed using a Hitachi S-3400N SEM on uncoated samples under low vacuum, and the elemental composition was determined via elemental mapping using EDX analysis (1,900 s scanning time at 15 keV, 62.0 μA and a working distance of 10 mm). After ToF-SIMS analysis, the samples were sputter-coated with gold and re-examined using a Zeiss Supra 40VP scanning electron microscope (2 keV, working distance 3–5 mm, Everhart–Thornley secondary electron detector).

**Time-of-flight secondary ion mass spectrometry.** ToF-SIMS is a chemical surface analysis technique in which mass spectra from the uppermost molecular layers of a sample are acquired through bombardment by a pulsed beam of high energy ions (primary ions). The collision of the primary ions with the sample surface results in the emission of molecules, molecular fragments and atoms, of which the ionised species (secondary ions) are extracted into a time-of-flight analyser for mass separation and detection. By focusing the primary ion beam onto a small spot and by scanning the beam over the surface, a mass spectrum is recorded from each raster point (pixel). The data collected can then be presented as either accumulated mass spectra from selected regions of interest within the analysis area, or as images showing the signal intensity distribution of specific secondary ions on the sample surface.

Molecular information pertaining to the sample surface can be obtained only if the measurement is taken under static conditions; that is, the collision between the primary ions and sample surface occurs at a spot where no previous collision has occurred. This condition is ensured by terminating the analysis well before a specific accumulated primary ion dose density is reached (termed the static limit), which is considered to be $10^{12}$–$10^{13}$ primary ions per $cm^2$.

The spatial resolution of the ToF-SIMS analysis is ultimately determined by the spot size of the primary ion beam, which for $Bi_3^+$ (the primary ion used in this study) can be focused to a diameter of about 100–200 nm. The mass resolution is determined by the precision by which the flight time of the secondary ions through the time-of-flight analyser can be resolved, which in turn is determined by the temporal pulse width of the primary ions as they hit the sample surface. As it is not possible to simultaneously obtain maximum spatial (narrow focus) and mass (short pulses) resolution without seriously sacrificing the primary ion current (and thereby the analysis time), ToF-SIMS analyses are normally conducted with the instrument optimised either for high mass resolution or for high spatial resolution.

In the present study, ToF-SIMS analyses in the static SIMS mode were performed in a ToF-SIMS IV instrument (IONTOF GmbH) using 25 keV $Bi_3^+$ primary ions and low energy electron flooding for charge compensation. High mass resolution data ($m/\Delta m \sim 5{,}000$) were acquired at a spatial resolution of ~3–4 μm, whereas high image resolution data (spatial resolution ~0.2–0.5 μm) were obtained at a mass resolution of $m/\Delta m \sim 300$; in both cases at 256 × 256 pixels. High mass resolution spectra were calibrated using the $C^-$, $C_2^-$, $C_2H^-$, $C_3^-$, and $C_4H^-$ peaks. Because the positive-ion spectra were found to show strong interference with the signal from the sedimentary matrix, only negative-ion data are presented here.

The overlay images presented in Figs 2b, 3b and 4b were produced with the open source software ImageJ (US National Institutes of Health; http://imagej.nih.gov/ij) after alignment of the ToF-SIMS and SEM figures using Adobe Photoshop Elements 9 (Adobe Systems). The spatial distribution of eumelanin-characteristic peaks; that is, $C_3N^-$, 50 u; $C_3NO^-$, 66 u; and $C_6H^-$, 73 u (see Extended Data Table 1), is shown in green in these three images. The spectra in Figs 2d, 3d and 4d were made in IGOR Pro 6.32A (WaveMetrics) and then redrawn using Adobe Illustrator 11.0.0 (Adobe Systems). Filled circles in these illustrations indicate the aforementioned peaks used to produce the eumelanin ion images in Figs 2b, 3b and 4b, whereas plus symbols indicate peaks from inorganic ions that are not part of the eumelanin structure (see comparison with synthetic eumelanin in Extended Data Fig. 5). In Figs 2d, 3d and 4d, the eumelanin spectrum is shifted (~0.4 u to the right) and the signal intensity adjusted relative to the fossil spectrum in order to facilitate detailed comparison (see also Extended Data Fig. 2). The close agreement between the fossil and eumelanin spectra (both with regard to their peak positions and intensity distributions) provides compelling evidence for a high eumelanin content on the surface of the melanosome-like microbodies forming the 'skin' in FUM-N-1450, SMU 76532 and YORYM 1993.338.

**Principal component analysis.** PCA was carried out using MATLAB v.7.1.0.246 (MathWorks) and PLS Toolbox v.4.0.2 (Eigenvector Research). The analysis included 57 peaks in the range 48–170 u, consisting of 43 major peaks from the synthetic eumelanin spectrum and 14 additional peaks from the (mostly) phaeomelanin spectrum (Extended Data Fig. 6). Corrected peak areas (signal intensities) were obtained from high mass resolution spectra using the SurfaceLab 6.3 software (ION-TOF GmbH). For each spectrum, the peak signal intensities were normalized to the total signal from all selected peaks. Normalized data were loaded into the PLS Toolbox software and auto-scaling was applied before analysis.

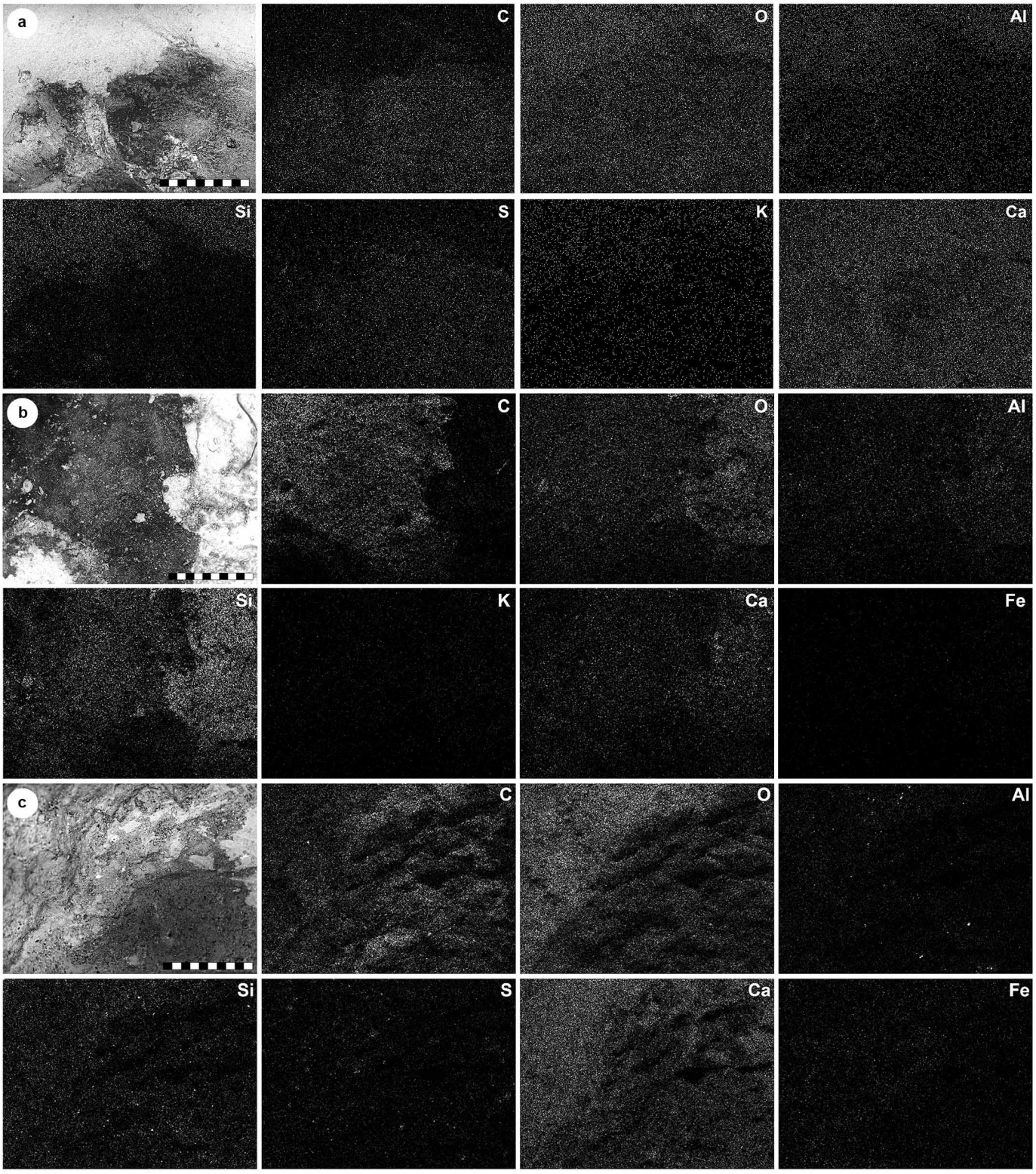


**Extended Data Figure 1 | Backscattered electron images and single-element EDX maps of fossil 'skin' samples.** **a**, Leatherback turtle *Eosphargis breineri*, FUM-N-1450. **b**, Mosasaur *Tylosaurus nepaeolicus*, SMU 76532. **c**, Ichthyosaur, YORYM 1993.338. Energy-dispersive X-ray (EDX) maps: white, high intensity; black, low intensity. Note relatively high levels of carbon (C) in the fossil 'skin' structures, represented by the dark region in the backscattered electron images. Scale bars, 1 mm.

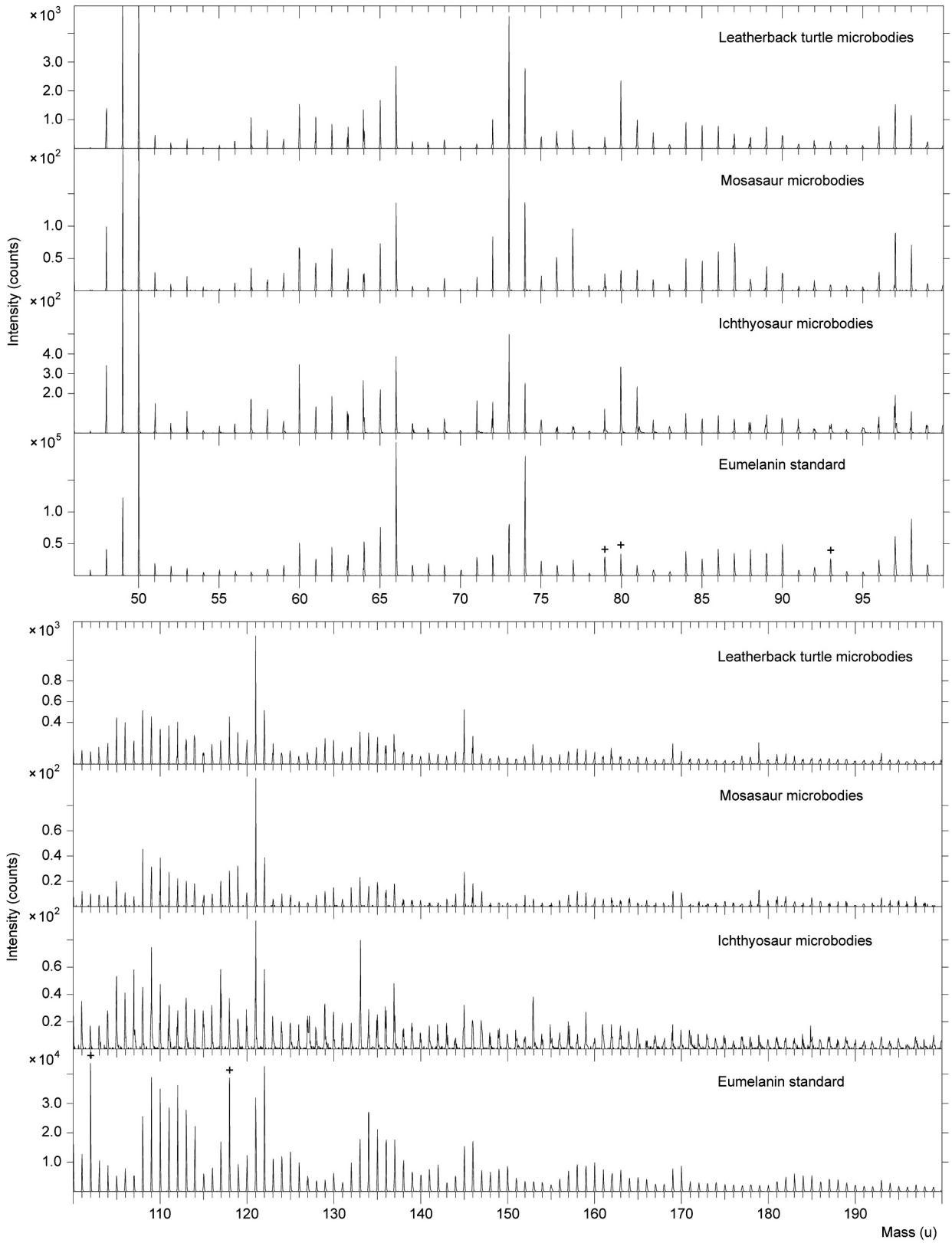


**Extended Data Figure 2 | Negative-ion ToF-SIMS spectra of 'skin' from FUM-N-1450, SMU 76532 and YORYM 1993.338, and natural eumelanin.** Note close agreement between fossil spectra, as well as between fossil spectra and that of the natural eumelanin standard (from *Sepia officinalis*). This similarity, both with regard to relative intensity distribution and precise mass of the eumelanin-related peaks in the entire mass range up to about 175 u (see also Extended Data Table 1), provides compelling evidence for high amounts of eumelanin pigment on the surface of the fossil microbodies. Differences in absolute signal intensities are caused by variations in instrument set up and data acquisition parameters, and are thus not related to the chemical composition of the samples. +, peaks in the natural eumelanin spectrum originating from impurities and not the eumelanin structure.

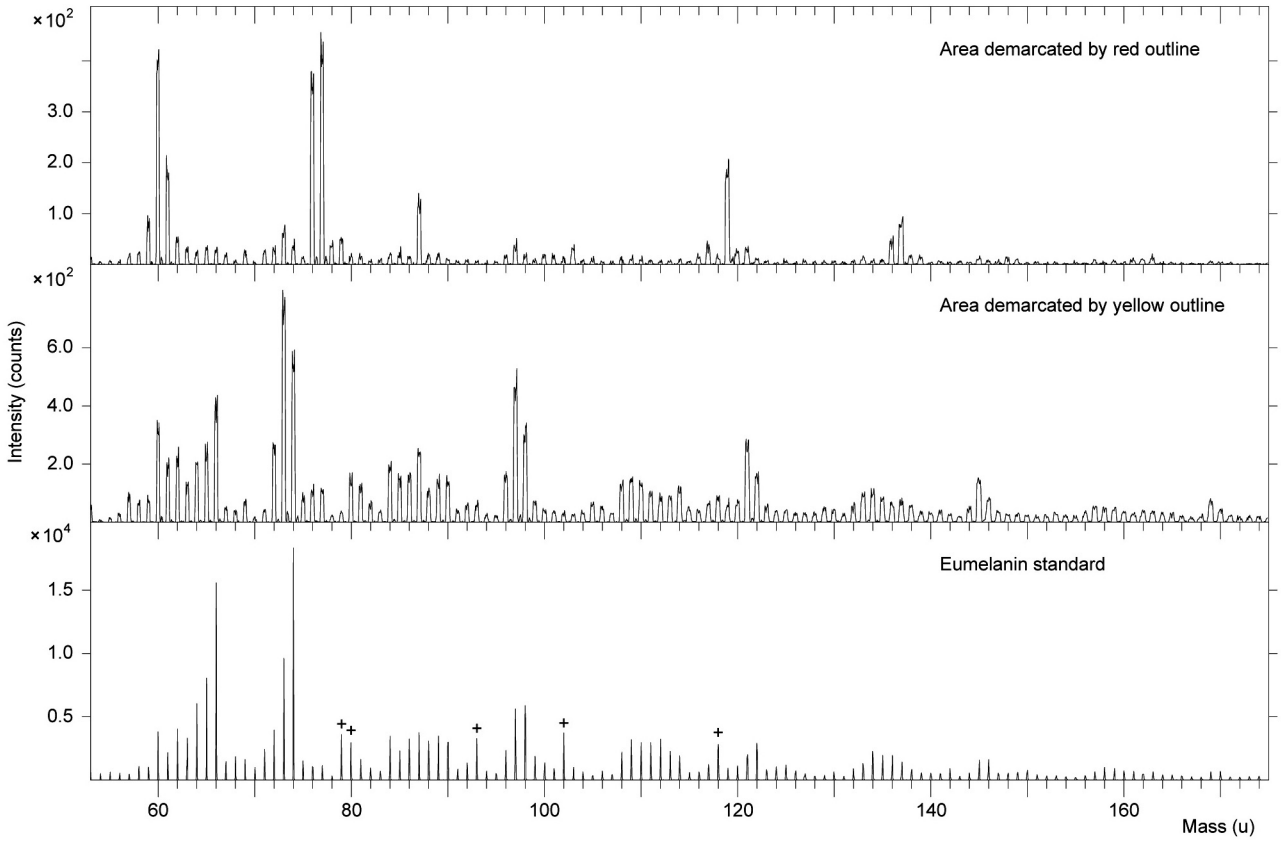


**Extended Data Figure 3 | Negative-ion ToF-SIMS spectra from selected regions of the mosasaur 'skin' sample together with natural eumelanin.** The spectra were obtained from an area containing primarily sedimentary matrix (top panel; red outline in Fig. 3b) and an area with abundant fossil melanosomes (middle panel; yellow outline in Fig. 3b). The spectrum acquired from the melanosome-rich area shows close agreement with the natural eumelanin standard spectrum (bottom panel), whereas the spectrum obtained from the sedimentary matrix is dominated by peaks representing ions of $Si_xO_y^-$ and $Si_xO_yH^-$ type, indicating silicate-rich minerals. Differences in peak widths are caused by variations in the data acquisition parameters and are thus not related to chemical composition. Specifically, the fossil spectra were acquired with the ToF-SIMS instrument optimised for high spatial resolution (resulting in broad peaks), whereas the eumelanin standard spectrum was acquired with the instrument optimised for high mass resolution (resulting in narrow peaks). +, peaks in the natural eumelanin standard spectrum originating from impurities and not the eumelanin structure.

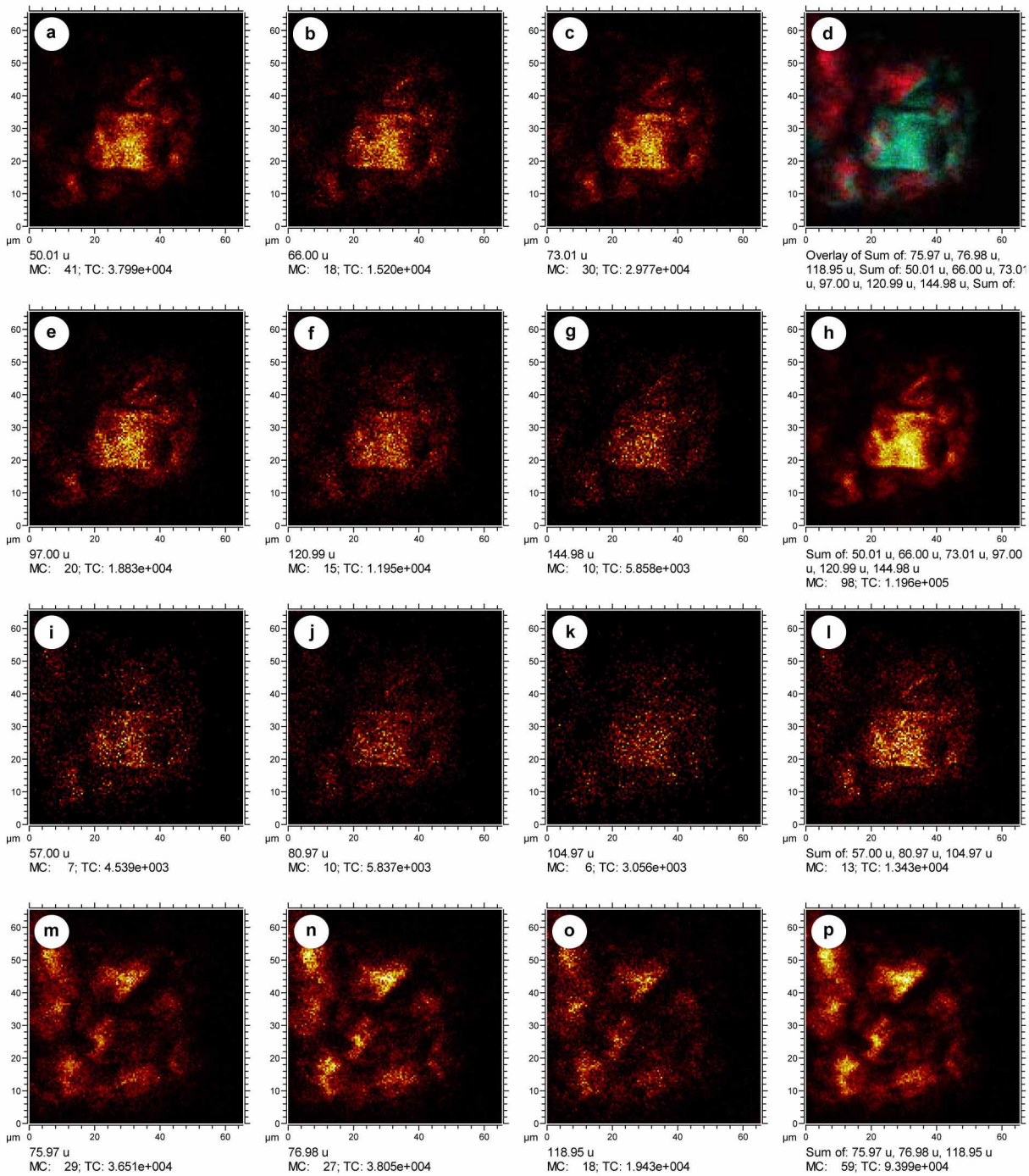


**Extended Data Figure 4 | Negative-ion ToF-SIMS images of peaks representing eumelanin, sulphur-containing organic fragments and silicon dioxide.** **a–p**, Peaks representing eumelanin (**a–c**, **e–h**), sulphur-containing organic fragments (**i–l**) and silicon dioxide (**m–p**). The data were collected from a single measurement of the mosasaur 'skin'. Note similar spatial distributions obtained for characteristic eumelanin peaks, sulphur-containing organic fragment peaks and silicon dioxide peaks, respectively. Note also comparable spatial distributions of eumelanin and sulphur-containing organic fragment peaks, suggesting diagenetic incorporation of sulphur with the eumelanin structure (Extended Data Fig. 6; see also Supplementary Information). Finally, note different spatial distribution of silicon dioxide peaks, representing the sedimentary matrix. The images in the right-hand column show the combined signal intensity for all peaks representing eumelanin (**h**), sulphur-containing organic fragments (**l**), silicon dioxide (**p**), and a colour overlay of these three images (**d**) in which green represents eumelanin, red represents silicon dioxide and blue represents sulphur-containing organic fragments. Peak mass is indicated beneath each image. MC, maximum count in one pixel; TC, total counts in the entire image.

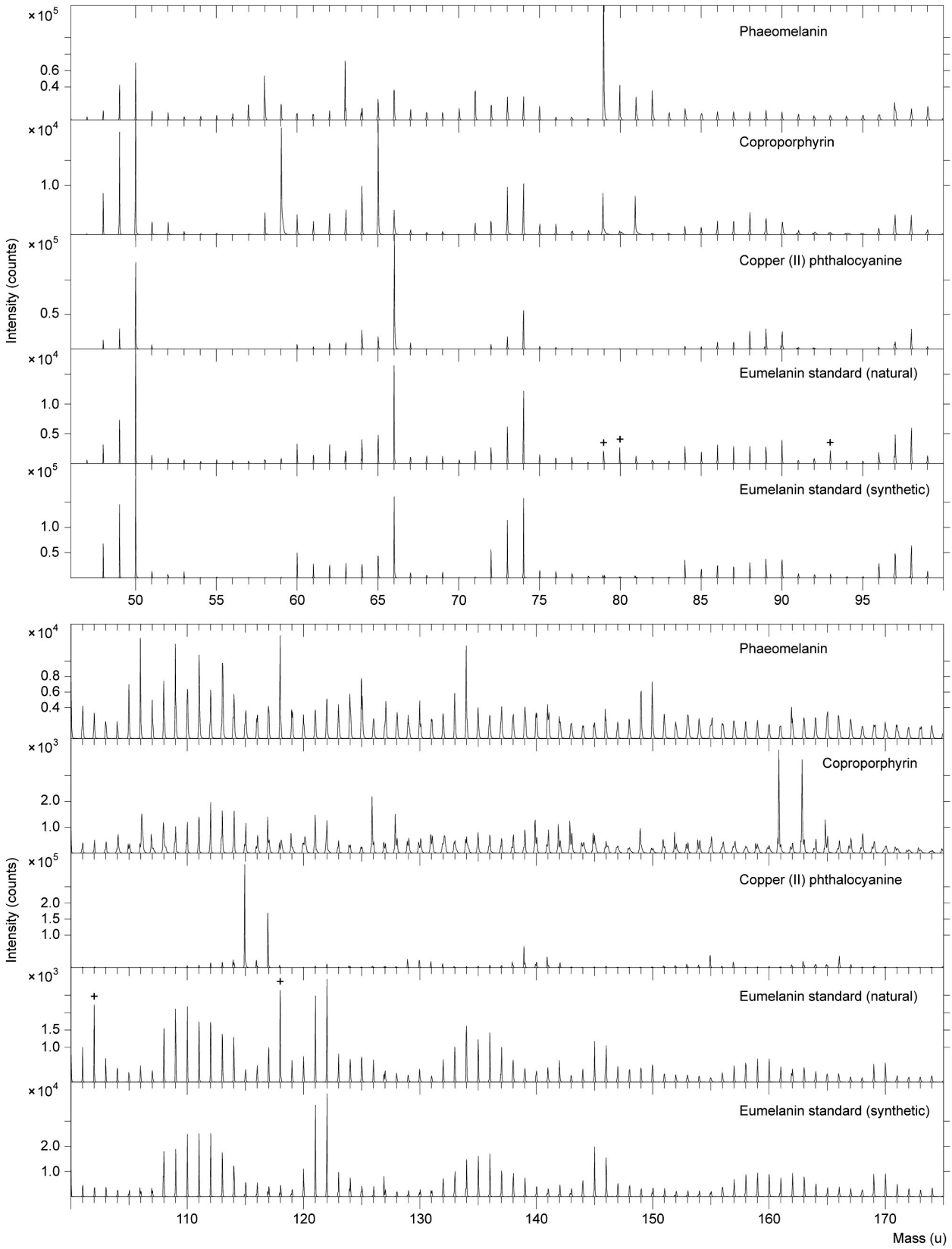


**Extended Data Figure 5 | Comparison of negative-ion ToF-SIMS spectra from compounds with a molecular structure similar to that of eumelanin.** Note that the two lower spectra (natural and synthetic eumelanin) are very similar to one another, with the only substantial differences relating to peaks representing impurities in the natural eumelanin standard (marked with +). The spectra from 'phaeomelanin' (see Supplementary Information) and the two porphyrins (coproporphyrin I dihydrochloride and copper (II) phthalocyanine) show some similarities with eumelanin in the mass range up to 100 u, although substantial differences also do occur. Above 100 u, the 'phaeomelanin' and porphyrin spectra lack several features that characterize the eumelanin spectra, including prominent peaks at 121, 122, 145 and 146 u.

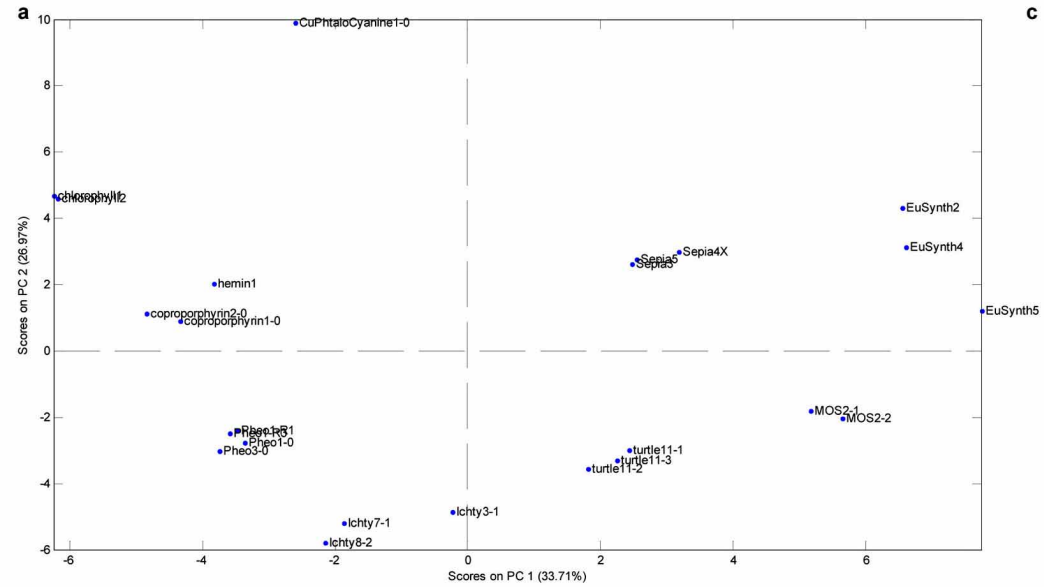


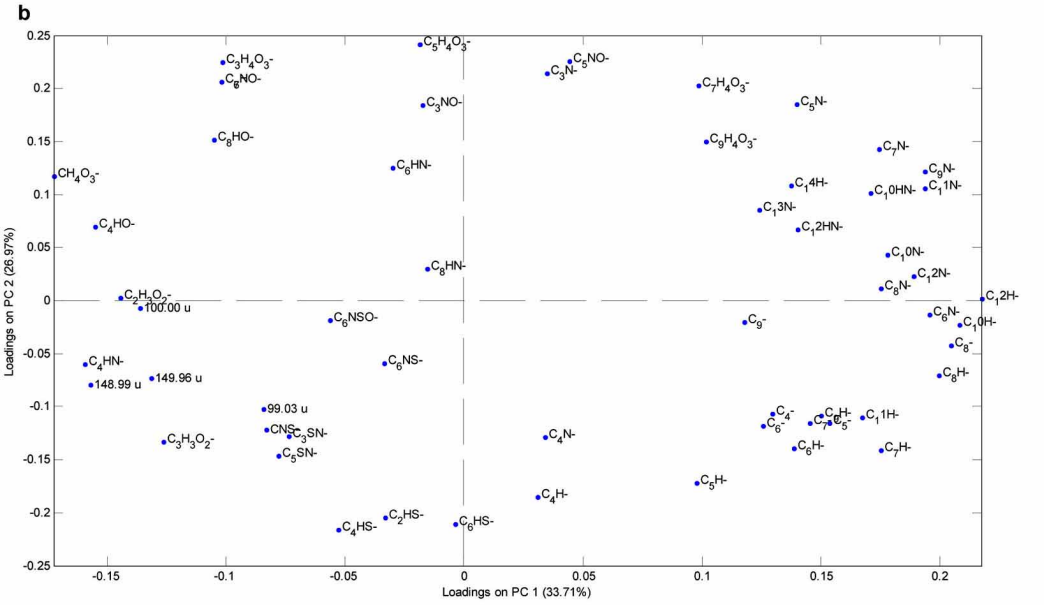


c

| Mass (u) | Assignment | Peak origin |
|---|---|---|
| 48.001 | $C_4^-$ | Eu |
| 49.010 | $C_4H^-$ | Eu |
| 50.006 | $C_3N^-$ | Eu |
| 56.984 | $C_2HS^-$ | Ph |
| 57.979 | $CNS^-$ | Ph |
| 59.019 | $C_2H_3O_2^-$ | Ph |
| 60.001 | $C_5^-$ | Eu |
| 61.009 | $C_5H^-$ | Eu |
| 62.013 | $C_4N^-$ | Eu |
| 63.015 | $C_4HN^-$ | Eu |
| 64.017 | $CH_4O_3^-$ | Eu |
| 65.014 | $C_4HO^-$ | Eu |
| 66.002 | $C_3NO^-$ | Eu |
| 71.023 | $C_3H_3O_2^-$ | Ph |
| 72.008 | $C_6^-$ | Eu |
| 73.007 | $C_6H^-$ | Eu |
| 74.007 | $C_5N^-$ | Eu |
| 80.975 | $C_4HS^-$ | Ph |
| 81.979 | $C_3SN^-$ | Ph |
| 84.008 | $C_7^-$ | Eu |
| 85.011 | $C_7H^-$ | Eu |
| 86.011 | $C_6N^-$ | Eu |
| 87.014 | $C_6HN^-$ | Eu |
| 88.016 | $C_3H_4O_3^-$ | Eu |
| 89.017 | $C_6HO^-$ | Eu |
| 90.002 | $C_5NO^-$ | Eu |
| 96.008 | $C_8^-$ | Eu |
| 97.007 | $C_8H^-$ | Eu |
| 98.009 | $C_7N^-$ | Eu |
| 99.025 | 99.03 u | Ph |
| 99.997 | 100.00 u | Ph |
| 104.981 | $C_6HS^-$ | Ph |
| 105.977 | $C_5SN^-$ | Ph |
| 107.995 | $C_9^-$ | Eu |
| 109.005 | $C_9H^-$ | Eu |
| 110.019 | $C_8N^-$ | Eu |
| 111.023 | $C_8HN^-$ | Eu |
| 112.016 | $C_5H_4O_3^-$ | Eu |
| 113.025 | $C_8HO^-$ | Eu |
| 114.021 | $C_7NO^-$ | Eu |
| 117.974 | $C_6NS^-$ | Ph |
| 121.006 | $C_{10}H^-$ | Eu |
| 122.000 | $C_9N^-$ | Eu |
| 133.009 | $C_{11}H^-$ | Eu |
| 133.968 | $C_6NSO^-$ | Ph |
| 134.010 | $C_{10}N^-$ | Eu |
| 135.006 | $C_{10}HN^-$ | Eu |
| 136.014 | $C_7H_4O_3^-$ | Eu |
| 145.009 | $C_{12}H^-$ | Eu |
| 146.003 | $C_{11}N^-$ | Eu |
| 148.992 | 148.99 u | Ph |
| 149.961 | 149.96 u | Ph |
| 158.001 | $C_{12}N^-$ | Eu |
| 159.010 | $C_{12}HN^-$ | Eu |
| 160.019 | $C_9H_4O_3^-$ | Eu |
| 169.009 | $C_{14}H^-$ | Eu |
| 170.004 | $C_{13}N^-$ | Eu |

**Extended Data Figure 6 | Principal component analysis comparing negative-ion ToF-SIMS spectra from our fossil samples, eumelanin, phaeomelanin and other molecular standards.** **a**, Score plot of principal component 1 (PC1) and PC2, in which each spectrum is represented by a data point. The position of each point reflects characteristic features of the spectrum. **b**, Loadings plot for PC1 and PC2, in which each point represents a specific peak included in the analysis. The position of each peak indicates that it has a relatively high signal intensity in the spectra located at a corresponding position in the score plot (and, conversely, that spectra located in other areas have relatively lower intensities of this particular peak). Note substantial separation between different samples and molecular compounds in the score plot (see Supplementary Information). **c**, Peaks included in the analysis. These were selected based on their prominence, as well as assignment to organic fragments in the synthetic eumelanin (Eu) and natural phaeomelanin (Ph) spectra, respectively (see Extended Data Fig. 5).

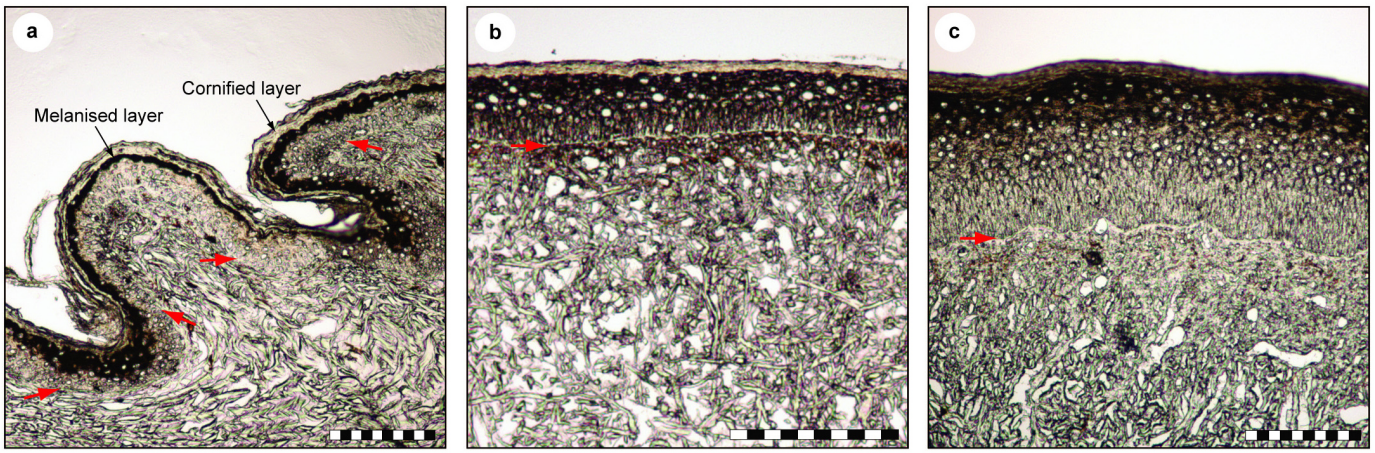


**Extended Data Figure 7 | Light micrographs of histological sections from unstained skin tissue of extant leatherback turtle, *Dermochelys coriacea*.** **a**–**c**, Sections taken from the hip region of a hatchling (Saint Croix, US Virgin Islands) (**a**), carapace of a juvenile (Palm Beach County, Florida, USA) (**b**) and periocular region of an adult (Hutchinson Island, Florida, USA) (**c**). Note the unusually dark melanised layer of the dermis directly under the cornified layer (red arrows denote basal membrane of epidermis). Samples had been fixed (within a few hours post mortem) in 10% buffered formalin for months (hip, periocular) to years (carapace), stored in 70% ethanol for approximately 3 and 22 years, respectively, and then embedded with Tissue-Tek O.C.T. Compound (Sakura Finetek) and sectioned into ~5-µm-thick slices using a Leica CM3050 S cryostat. Samples were transported to R.M.C. under authorisation of the US Fish and Wildlife Service with approval from the Florida Fish and Wildlife Conservation Commission pursuant to Marine Turtle Permit no. 073. Scale bars, 100 µm.

**Extended Data Figure 8 | Fossil ichthyosaur *Stenopterygius quadriscissus* with preserved body outline.** Note full 'skin' envelope preserved as amorphous black material (PMU R435; Museum of Evolution, Uppsala, Sweden), indicating that the animal was uniformly dark-coloured in life. Scale bar, 5 cm.

**Extended Data Table 1 | Tentative assignment and position of eumelanin peaks in negative-ion ToF-SIMS spectra of two eumelanin standards (synthetic and natural *Sepia*) and the fossil 'skin' samples examined in this work**

| Tentative assignment | Theoretical mass (u) | Synthetic eumelanin | Natural eumelanin | FUM-N-1450 | SMU 76532 | YORYM 1993.338 |
|---|---|---|---|---|---|---|
| $C_4^-$ | 48.000 | 48.000 | 48.001 | 48.001 | 48.001 | 48.001 |
| $C_4H^-$ | 49.008 | 49.010 | 49.010 | 49.010 | 49.011 | 49.010 |
| $C_3N^-$ | 50.003 | 50.007 | 50.005 | 50.006 | 50.007 | 50.006 |
| $C_5^-$ | 60.000 | 60.002 | 60.002 | 60.001 | 60.002 | 60.000 |
| $C_5H^-$ | 61.007 | 61.008 | 61.009 | 61.009 | 61.013 | 61.010 |
| $C_4HO^-/H_3NO_3^-$ | 65.003/65.012 | 65.009 | 65.013 | 65.008 | 65.012 | 65.008 |
| $C_3NO^-$ | 65.998 | 66.003 | 66.001 | 66.001 | 66.004 | 66.002 |
| $C_6^-$ | 72.000 | 72.001 | 72.003 | 72.001 | 72.002 | 72.002 |
| $C_6H^-/C_2H_3NO_2^-$ | 73.008/73.016 | 73.010 | 73.010 | 73.010 | 73.013 | 73.011 |
| $C_3N^-/C_2H_2O_3^-$ | 74.003/74.001 | 74.006 | 74.006 | 74.006 | 74.007 | 74.007 |
| $C_7^-$ | 84.000 | 84.000 | 84.002 | 84.000 | 84.004 | 84.001 |
| $C_7H^-$ | 85.008 | 85.008 | 85.010 | 85.009 | 85.013 | 85.009 |
| $C_6N^-/C_7H_2^-$ | 86.003/86.015 | 86.009 | 86.009 | 86.013 | 86.013 | 86.015 |
| $C_6HN^-$ | 87.011 | 87.015 | 87.014 | 87.015 | 87.027 | 87.016 |
| $C_6H_2N^-/C_3H_4O_3^-$ | 88.018/88.016 | 88.015 | 88.014 | 88.016 | 88.016 | 88.020 |
| $C_6HO^-/C_2H_3NO_3^-$ | 89.002/89.011 | 89.012 | 89.015 | 89.011 | 89.012 | 89.015 |
| $C_2NO^-$ | 89.998 | 90.003 | 90.002 | 90.002 | 90.005 | 90.004 |
| $C_8^-$ | 96.000 | 95.999 | 96.002 | 95.999 | 96.004 | 96.000 |
| $C_8H^-/C_4H_3NO_2^-$ | 97.008/97.016 | 97.009 | 97.010 | 97.009 | 97.012 | 97.010 |
| $C_7N^-/C_4H_2O_3^-$ | 98.003/98.001 | 98.005 | 98.006 | 98.005 | 98.012 | 98.008 |
| $C_9^-$ | 108.000 | 107.999 | 107.999 | 107.989 | 107.996 | 107.986 |
| $C_9H^-$ | 109.008 | 109.008 | 109.004 | 109.006 | 109.010 | 109.009 |
| $C_8N^-/C_9H_2^-$ | 110.003/110.015 | 110.009 | 110.010 | 110.011 | 110.018 | 110.015 |
| $C_8HN^-$ | 111.011 | 111.015 | 111.015 | 111.013 | 111.020 | 111.017 |
| $C_8H_2N^-/C_5H_4O_3^-$ | 112.019/112.016 | 112.016 | 112.015 | 112.015 | 112.015 | 112.022 |
| $C_8HO^-/C_4H_3NO_3^-$ | 113.003/113.012 | 113.017 | 113.017 | 113.011 | 113.015 | 113.009 |
| $C_7NO^-$ | 113.999 | 114.002 | 114.006 | 113.988 | 113.976 | 113.993 |
| $C_{10}^-$ | 120.000 | 120.000 | 119.996 | 119.997 | 119.993 | 120.006 |
| $C_{10}H^-/C_6H_3NO_2^-$ | 121.008/121.016 | 121.008 | 121.010 | 121.006 | 121.015 | 121.010 |
| $C_9N^-$ | 122.004 | 122.005 | 122.006 | 122.004 | 122.010 | 122.005 |
| $C_{12}H^-/C_8H_3NO_2^-$ | 145.008/145.016 | 145.006 | 145.009 | 145.005 | 145.010 | 145.003 |
| $C_{11}N^-$ | 146.003 | 146.006 | 146.007 | 146.002 | 146.005 | 146.012 |

The fossil 'skin' samples were obtained from a leatherback turtle (FUM-N-1450), a mosasaur (SMU 76532) and an ichthyosaur (YORYM 1993.338).

doi:10.1038/nature12899

**Specimen details**

•FUM-N-1450 is the holotype of *Eosphargis breineri* Nielsen, 1959, and it includes the articulated remains of a large-sized (estimated total body length ~1.5 m) leatherback turtle. The specimen was collected at the Knudeklint locality on the Island of Fur in northern Jutland, Denmark[S1,S2]. The fossil is preserved in calcareous concretions originating from the stratigraphic level 'ash layer minus 33' of the Fur Formation[S3]. This particular deposit has been associated with the Island of Lundy eruption in the Bristol Chanel[S3], and its age has been estimated to be about 55 Ma (Early Eocene)[S4]. Because the fossil-bearing nodules were found embedded in ash, it is conceivable that the turtle perished from suffocation during the eruption event, a scenario that also may explain the absence of bite marks and scratches inflicted by scavenging bony fish and/or sharks. Presumably, the carcass ended up in the anoxic bottom sediments, tilted somewhat to the left, and subsequently was encased in three lens-shaped nodules comprising the rear of the animal, the anterior left of the trunk, and the skull, respectively. Blackish soft tissue matter was found in the concretion containing the posterior part of the turtle, and appears to originate from the area between the left hind limb and anus. FUM-N-1450 has not been treated with any preservative or consolidant.

•SMU 76532 consists of a semi-articulated skeleton (preserved portion ~11 m in length) assigned to the tylosaurine mosasaur *Tylosaurus nepaeolicus*[S5]. The specimen was found approximately 1.6 km southeast of Terlingua ghost town in the Late Coniacian (~86 Ma) San Vicente Member of the Boquillas Formation. Portions of the skull, including the diagnostic quadrates, were recovered along with a number of trunk vertebrae, part of the anterior tail, pelvic girdle, and hind limb elements associated with a scattering of smaller materials representing stomach contents (including the durophagous shark *Ptychodus mortoni* and another mosasaur referred to the plioplatecarpine genus *Platecarpus*[S5]). An articulated section of rhomboidal 'scales' (~40 × 35 mm) preserved as matt blackish material was discovered during the excavation of SMU 76532. The 'scales' are relatively uniform in size (measuring 1.5–2.3 mm in length and 2.0–2.6 mm in width), and obliquely arrayed into an alternating pattern. The slab preserving the 'scales' was originally treated with very thin polyvinyl butyral dissolved in acetone; however, further preparations in 2012 uncovered an area with untreated 'scales'. Both treated and untreated 'scales' were examined in this study. Data from the latter are presented in Fig. 3 and Extended Data Figs 2 and 3.

•YORYM 1993.338 consists of an essentially articulated section of ichthyosaur caudal vertebrae (overall length of segment ~21 cm) with associated soft tissues preserved as blackish material, found in a calcareous concretion from the Sinemurian (~196–190 Ma) of Black Ven, Dorset, England (see ref. 11 for details). Even though the fossil preserves in exquisite detail the outline of a lunate tail fin in left lateral view, it has not been possible to confidently assign it to a particular genus or species[11]. YORYM 1993.338 was mechanically prepared without application of preservatives.

**Fossil melanosome measurements**

•FUM-N-1450: mean length = 812.6 nm [number measured (*n*) = 75, standard deviation (SD) = 195.7, min = 450.4, max = 1439.0], mean width = 467.8 nm (*n* = 75, SD = 88.7, min = 278.4, max = 674.3).

•SMU 76532: mean length = 504.9 nm (*n* = 75, SD = 125.8, min = 207.6, max = 808.9), mean width = 323.0 nm (*n* = 75, SD = 66.5, min = 184.4, max = 523.3).

•YORYM 1993.338: mean length = 778.5 nm (*n* = 75, SD = 192.2, min = 409.8, max = 1245.1), mean width = 483.9 nm (*n* = 75, SD = 97.1, min = 318.8, max = 651.3).

**Additional material examined**

In addition to the fossil specimens described above, the following molecules and structures were examined in this study (a selection of spectra from compounds with a molecular structure similar to that of eumelanin is presented in Extended Data Fig. 5):

***Melanins***

- Natural eumelanin from the cephalopod *Sepia officinalis* (Sigma-Aldrich).
- Natural melanin (mostly phaeomelanin) from feathers of the Rhode Island Red chicken, *Gallus gallus domesticus* (extracted according to protocol in ref. S6).
- Synthetic eumelanin (Fisher Scientific).

***Chromatophore compounds***

- Xanthophyll from marigold (Sigma-Aldrich).
- Guanine (Sigma-Aldrich).
- Isoxanthopterin (Sigma-Aldrich).
- Riboflavin (Sigma-Aldrich).

***Porphyrins***

- Coproporphyrin I dihydrochloride (Sigma-Aldrich).
- Hemin chloride (MP Biomedicals).
- Chlorophyll *a* from *Anacytis nidulans* (Sigma-Aldrich).

***Compounds structurally similar to melanin***

- Copper (II) phthalocyanine (Sigma-Aldrich).
- Copper (II) acetylacetonate (Sigma-Aldrich).

***Microbial mat samples***

These were obtained from a methane seep on the NW Black Sea shelf (one sample)[S7] and from rock surfaces in the Tunnel of Äspö (Äspö Hard Rock Laboratory, SE Sweden; two samples from sites located at 2,200 and 3,440 m from the tunnel entrance, respectively). The Black Sea sample is largely comprised of methanotrophic archaea, whereas the Äspö mats represent phototrophic systems with abundant cyanobacteria. The microbial mats were analysed as cryosections, as previously described[S7]. For spectral data, see ref. 16.

**Spectral differences between fossil 'skin' samples and melanin standards**

Although our ToF-SIMS analyses demonstrate a detailed agreement between the spectra acquired from the three fossil 'skin' samples and the two eumelanin standards, including major peaks at 49, 50, 66, 73, 74, 97, 98, 121, 122, 145, and 146 u, substantial differences also do occur. The latter are mainly of two types (Extended Data Fig. 2):

(i) A substantially increased signal from peaks corresponding to sulphur-containing organic fragments of $C_nHS^-$-type, where n = 2 (57 u), 4 (81 u) and 6 (105 u), in the fossil spectra compared to the natural eumelanin spectrum (the synthetic eumelanin spectrum shows no substantial signal from these peaks).

(ii) A consistently lower signal from peaks corresponding to $C_nN^-$, where n = 3 (50 u), 5 (74 u), 7 (98 u), 9 (121 u), and 11 (146 u), in relation to the preceding peak; that is, $C_nH^-$, where n = 4 (49 u), 6 (73 u), 8 (97 u), 10 (120 u), and 12 (145 u), in the fossil spectra compared to the natural eumelanin spectrum.

The natural 'phaeomelanin' spectrum (Extended Data Fig. 5) displays prominent peaks assignable to sulphur-containing organic fragments, including $C_nHS^-$ [where n = 2 (57 u), 4 (81 u) and 6 (105 u)], $C_nNS^-$ [where n = 1 (58 u), 3 (82 u), 5 (106 u), and 6 (118 u)] and $C_6NSO^-$ (134 u), in addition to unidentified peaks with elevated intensities occurring at 99, 100, 149, and 150 u, respectively (peaks at 63 and 79 u belong to phosphate-containing impurities). Substantial signal from characteristic eumelanin peaks is also present in the 'phaeomelanin' spectrum in the mass range < 100 u, and the peaks show a relative intensity distribution similar to that of the natural eumelanin spectrum. This is likely a consequence of

eumelanin impurities in the extracted 'phaeomelanin' sample (almost all extant avian melanosomes contain a mixture of eu- and phaeomelanin[29]).

Spectral differences between our samples were evaluated by principal component analysis (PCA). Extended Data Fig. 6 shows a score plot and a loadings plot from a PCA analysis that includes our three fossil 'skin' samples, different melanins and a selection of other molecular standards (compounds showing few spectral similarities with eumelanin and/or the fossil samples were not included in the analysis). A total of 57 peaks, selected from the synthetic eumelanin (43) and 'phaeomelanin' (14) spectra, were included in the analysis (Extended Data Fig. 6c). The score plot shows distinct separations between the various samples (Extended Data Fig. 6a), indicating substantial spectral differences. Characteristics of these dissimilarities are visualised in the loadings plot (Extended Data Fig. 6b). The position of each peak indicates that it has a relatively high signal intensity in spectra located at a corresponding position in the score plot (and, conversely, that spectra located in other areas have relatively lower intensities of this particular peak). The score plot shows the eumelanin standards associated with the mosasaur and leatherback turtle spectra to the right (positive PC1 scores), whereas 'phaeomelanin' and the other standards are located to the left (negative PC1 score). The ichthyosaur spectra are positioned in the lower central part of the diagram (negative PC2 score). Close inspection of the loadings plot shows that with the exception of the $C_nHS^-$ peaks, the 'phaeomelanin' peaks are all localised to the region of the 'phaeomelanin' spectra in the score plot. The $C_nHS^-$ peaks are, on the other hand, located in the region of the ichthyosaur spectra, indicating that these peaks are particularly strong in that sample. Comparison between the 'phaeomelanin' and ichthyosaur spectra (both directly and in the PCA analysis) thus shows that it is mainly $C_nHS^-$-related peaks occurring in the ichthyosaur spectra, while the other 'characteristic' 'phaeomelanin' peaks show much lower signal intensities in the ichthyosaur spectra than would be expected had they been derived from this biochrome. When comparing the fossil spectra with one another, their relative positions in the score plot indicate an increasing $C_nHS^-$ signal in the order: mosasaur < leatherback turtle < ichthyosaur.

Even though we cannot exclude minor contributions from phaeomelanin pigment in the fossil 'skin' spectra due to the presence of sulphur, the results from our PCA analysis suggest that the sulphur-containing fragment ions originate largely from another source, presumably the diagenetic incorporation of sulphur with the eumelanin molecule[S8]. This hypothesis is corroborated by: (1) the co-localisation of sulphur-containing fragment peaks [$C_nHS^-$, where n = 2 (57 u), 4 (81 u) and 6 (105 u)] with eumelanin peaks in the ion images (Extended Data Fig. 4); and (2) the fact that these peaks are also present in the natural eumelanin spectrum, albeit at lower relative intensities when compared to the fossil spectra (Extended Data Fig. 2). *Sepia* melanin is generally considered to be pure eumelanin[S9], and although the origin of sulphur atoms in modern eumelanin pigments is not fully understood[S10,S11], sulphur incorporation is nonetheless possible[S10]. Additionally, as stated above, the other 'characteristic' 'phaeomelanin' peaks show much lower signal intensities in the ichthyosaur spectra than would be expected had they instead been derived from phaeomelanin. Hence, the relatively close localisation of the 'phaeomelanin' and ichthyosaur spectra in the score plot (Extended Data Fig. 6a) is by all likelihood a combination of: (1) eumelanin residues in the modern 'phaeomelanin' spectrum; and (2) diagenetically induced sulphur incorporation with the fossil eumelanin structure.

Compared to the eumelanin standard spectra, the fossil spectra are all located in the lower part of the score plot (lower PC2 scores). Examination of the eumelanin region in the loadings plot (positive PC1 scores) thus provides information regarding differences in relative intensity distribution of the eumelanin peaks between the eumelanin standards and fossil samples. For instance, it is readily apparent that peaks assigned to $C_nN^-$, where n = 3, 5, 7, 9,

11, and 13, are located in the upper part of the loadings plot (positive PC2 loadings), suggesting that these peaks are strong in the eumelanin spectra relative to the fossil spectra. Similarly, peaks assigned to $C_nH^-$, where n = 4, 6, 8, and 10, are located in the lower part of the loadings plot (negative PC2 loadings), indicating that these peaks are relatively strong in the spectra acquired from the fossil samples. Because these differences appear consistently, they presumably reflect minor modifications of the eumelanin molecular structure during diagenesis.

**Rationale for assignment of microstructures to fossilised melanosomes**

Although some microbes are able to produce melanin[S12–S14], we find it highly unlikely that the eumelanin-containing structures we identified in three phylogenetically diverse specimens all represent decomposed prokaryote mats[7,13,S15], because the pigment is associated with integument consistent with significant melanisation in living reptiles (Extended Data Fig. 7)[3,4,S16]. The fossil microbodies presented herein are also solid with a seemingly homogenous internal content (Fig. 3c, arrowheads), similar to melanosomes of extant organisms[17]. Conversely, purified bacterial melanins form amorphous deposits[S17], due to the fact that melanin production generally occurs extracellularly in these microbes[S14], and melanin is usually localised to the cell wall in eukaryotic microorganisms, resulting in hollow structures (so-called 'melanin ghosts'[S12–S14]). Furthermore, melanised microbe ghosts frequently display crater-like bud scars[S12,S13], marks that are absent on the surface of the ancient eumelanin-containing microbodies. Hence, we conclude that the microstructures preserved in FUM-N-1450, SMU 76532 and YORYM 1993.338 are the fossilised remains of endogenous pigment organelles.

It has previously been shown that multimillion-year-old melanosomes contain almost exclusively melanin, suggesting that other biomolecules, such as proteins and lipids, are lost during the process of fossilisation[16]. In extant animals, melanosomes develop in specialised pigment cells (melanophores/melanocytes) through four morphologically distinct stages and melanin deposition increases with organelle maturation[S18]. Thus, it is reasonable to assume that fully melanised melanosomes are more likely to be retained in the fossil record, and that the complex, cross-linked polymeric structure of melanin prevents these colour-producing organelles from disintegrating despite an absence of lipids and structural proteins in their fossilised state. However, some slight alterations in size and geometry may have occurred, and are presumably the effects of temperature and pressure during burial[S19].

Finally, it should be pointed out that the taphonomy of skin is different from that of feathers[S20], as is the deposition of melanin within each of these tissues[S21]; it is currently unknown what effects these factors may have on the mechanism(s) and likelihood of melanin preservation in the fossil record.

**Supplementary references**

S1. Nielsen, E. Eocene turtles from Denmark. *Meddelelser fra Dansk Geologisk Forening* **14,** 96–115 (1959).

S2. Nielsen, E. On the post-cranial skeleton of *Eosphargis breineri* Nielsen. *Meddelelser fra Dansk Geologisk Forening* **15,** 281–313 (1963).

S3. Larsen, L. M., Fitton, J. G. & Pedersen, A. K. Paleogene volcanic ash layers in the Danish Basin: compositions and source areas in the North Atlantic Igneous Province. *Lithos* **71,** 47–80 (2003).

S4. Morton, A. C. & Evans, J. A. Geochemistry of basaltic ash beds from the Fur Formation, Island of Fur, Denmark. *Bull. Geol. Soc. Denmark* **37,** 1–9 (1988).

S5. Bell, Jr. G. L., Barnes, K. R. & Polcyn, M. J. Late Cretaceous mosasauroids (Reptilia, Squamata) of the Big Bend region in Texas, USA. *Earth Environ. Sci. Trans. R. Soc. Edinburgh* **103,** 571–581 (2013).

S6. Liu, Y. *et al*. Comparison of the structural and physical properties of human hair eumelanin following enzymatic or acid/base extraction. *Pigm*. *Cell Res*. **16,** 355–365 (2003).
S7. Thiel, V. *et al*. Biomarkers at the microscopic range: ToF-SIMS molecular imaging of Archaea-derived lipids in a microbial mat. *Geobiology* **5,** 413–421 (2007).
S8. McNamara, M. E. *et al*. High-fidelity organic preservation of bone marrow in ca. 10 Ma amphibians. *Geology* **34,** 641–644 (2006).
S9. Glass, K. *et al*. Direct chemical evidence for eumelanin pigment from the Jurassic period. *Proc*. *Natl*. *Acad*. *Sci*. **109,** 10218–10223 (2012).
S10. Jimbow, K. *et al*. Characterization of melanogenesis and morphogenesis of melanosomes by physicochemical properties of melanin and melanosomes in malignant melanoma. *Cancer Res*. **44,** 1128–1134 (1984).
S11. Prota, G. *Melanins and Melanogenesis* (Academic Press, 1992).
S12. Nosanchuk, J. D. & Casadevall, A. The contribution of melanin to microbial pathogenesis. *Cell*. *Microbiol*. **5,** 203–223 (2003).
S13. Eisenman, H. C. *et al*. Microstructure of cell wall-associated melanin in the human pathogenic fungus *Cryptococcus neoformans*. *Biochemistry* **44,** 3683–3693 (2005).
S14. Plonka, P. M. & Grabacka, M. Melanin synthesis in microorganisms – biotechnological and medical aspects. *Acta Biochim*. *Polon*. **53,** 429–443 (2006).
S15. Martill, D. M. Soupy substrates: a medium for the exceptional preservation of ichthyosaurs of the Posidonia Shale (Lower Jurassic) of Germany. *Kaupia* **2,** 77–97 (1993).
S16. Bechtel, H. B. Color and pattern in snakes (Reptilia, Serpentes). *J*. *Herpetol*. **12,** 521–532 (1978).
S17. Tarangini, K. & Mishra, S. Production, characterization and analysis of melanin from isolated marine *Pseudomonas* sp. using vegetable waste. *Res*. *J*. *Eng*. *Sci*. **2,** 40–46 (2013).
S18. Wasmeier, C., Hume, A. N., Bolasco, G. & Seabra, M. C. Melanosomes at a glance. *J*. *Cell Sci*. **121,** 3995–3999 (2008).
S19. McNamara, M. E., Briggs, D. E. G., Orr, P. J., Field, D. J. & Wang, Z. Experimental maturation of feathers: implications for reconstructions of fossil feather colour. *Biol*. *Lett*. **9,** 20130184 (2013).
S20. Schweitzer, M. H. Soft tissue preservation in terrestrial Mesozoic vertebrates. *Annu*. *Rev*. *Earth Planet*. *Sci*. **39,** 187–216 (2011).
S21. Lucas, A. M. & Stettenheim, P. R. *Avian Anatomy: Integument* (US Department of Agriculture, 1972).